Supplementary Information for

Lattice Chloride Doping-induced d-band modulation in Cu_2O Nanocubes for Efficient Electrocatalytic Biomass Oxidation

Xuchen Zheng,[1] Jiaojiao Wu,[1] Shenze Ding,[1] Qiuyan Jin,[1] Yurui Xue,[2] Xiangya Xu[1]*

[1]Department of Catalytic Science, SINOPEC Beijing Research Institute of Chemical Industry, Co., Ltd, Beijing, P. R. China.

[2]State Key Laboratory of Supramolecular Structure and Materials, College of Chemistry, Jilin University, Changchun, China

Materials.

Potassium chloride and copper sulfate pentahydrate were brought from Energy. 5-hydroxymethyl furfural (HMF) was purchased from Alfa Aesar. KOH was purchased from Macklin. The water used in all experiments was purified with a Millipore system. All the chemicals were of chemical grade and were used as received without further purification.

Methods

Preparation of Cl-Cu_2O NC. Typically, 11.2 mg potassium chloride and 37.5 mg copper sulfate pentahydrate were added to the 30mL H_2O. The solution was thoroughly mixed as the subsequent electrolyte. Cl-Cu_2O NC was electrodeposited by cyclic voltammetry (CV) in a single cell with three-electrode system. The carbon paper was used as the working electrode. The Pt (1 cm × 1 cm) and the saturated calomel electrodes were used as the counter electrode and the reference electrode, respectively. Cyclic Voltammetry scans were conducted at -0.55 V to 0.05 V vs. SCE with the scanning speed of 5 mV s^{-1} in 40 mins. After eletrodeposition, the Cl-Cu_2O NC/carbon paper was washed with deionized water and dried under Ar flow.

Preparation of Cu_2O NC. Typically, given amounts of 0.556 g PVP and 0.1 g sodium citrate was first dissolved in 100 mL of DI water, and 0.171 g of $CuCl_2$·2H2O was added into the above solution. Then, 10 mL NaOH aqueous solution (2 M) was added dropwise (1 drop/s) into the above mixture solution with continuous stirring for 0.5 h. Finally, 10 mL of l-ascorbic acid aqueous solution (0.6 M) was added dropwise and the mixture was aged for 3 h before being centrifuged at 9000 rpm for 5 min. All of these procedures were carried out in a water bath at 55 °C.

Preparation of Cu_2O Oct. Typically, given amounts of 8.8 g PVP and 0.1 g sodium citrate was first dissolved in 100 mL of DI water, and 0.171 g of $CuCl_2$·2H2O was added into the above solution. Then, 10 mL NaOH aqueous solution (2 M) was added dropwise (1 drop/s) into the above

mixture solution with continuous stirring for 0.5 h. Finally, 10 mL of l-ascorbic acid aqueous solution (0.6 M) was added dropwise and the mixture was aged for 3 h before being centrifuged at 9000 rpm for 5 min. All of these procedures were carried out in a water bath at 55 °C.

Preparation of $Cu(OH)_2$. Typically, $Cu(OH)_2$ nanowires grew on the Cu foil in situ by immersing the sensor in NaOH (0.375 M) and $(NH)_4S_2O_8$ (0.015 M) aqueous solution at 25 °C, followed by being rinsed with deionized water and ethanol sequentially.

Characterizations

Scanning electron microscopy (SEM) images were collected by an S-4800 field emission scanning electron microscope. Transmission electron microscopy (TEM), high-resolution TEM (HRTEM) images and energy-dispersive X-ray spectroscopy (EDS) were recorded on a JEM-2100F electron microscope operating at 200 kV. AFM images were recorded using Bruker FASTSCANBIO at room temperature under non-contact mode. X-ray diffraction (XRD) was conducted on a Japan Rigaku D/max-2500 rotation anode X-ray diffractometer using Cu Kα radiation (λ = 1.54178 Å). Raman spectra were obtained by a Renishaw-2000 Raman spectrometer exploiting a 514.5 nm excitation laser source. The X-ray photoelectron spectroscopy (XPS) data were obtained by a Thermo Scientific ESCA Lab 250Xi instrument with monochromatic Al Kα X-ray radiation. The in-situ infrared (IR) spectra were recorded at a resolution of 2 cm^{-1} on a Bruker Vertex 70v vacuum micro-Fourier infrared spectrometer, scanning from 4000 to 400 cm^{-1} at room temperature. Product quantification was determined by high-performance liquid chromatography (HPLC, Agilent 1260) with a UV-Vis detector set at 254 nm. HPLC was equipped with a C18 column (4.6 mm × 100 mm, Shim-pack GIST 5-μm).

Electrochemical Measurements

Electrochemical measurements were performed on a CHI-760E electrochemical workstation (CHI)

in an H-type cell with three-electrode system. The as-prepared catalyst was used as the working electrode. The Pt (1 cm × 1 cm) and the saturated calomel electrodes were used as the counter electrode and the reference electrode, respectively. All measurements were performed at room temperatures in electrolytes which were pretreated by bubbling Ar flow for 1 h. The electrochemically active surface area (ECSA) was measured by the double layer capacitance method. Cyclic Voltammetry (CV) scans were conducted at non-Faradaic potential range. All potentials were convert the reversible hydrogen electrode (RHE) according to the equation: $E_{RHE} = E_{SCE} + E_{0SCE} + 0.059pH$.

Computational details.

All the density functional theory (DFT) calculations were carried out using the Vienna Ab initio Simulations Package (VASP). The GGA-PBE exchange-correlation functional was used, and the interactions between ion cores and valence electrons were described following the projector augmented wave (PAW) approach. The one-electron wavefunction was developed using a plane-wave basis set with a cutoff energy of 400 eV. Reciprocal space was sampled using Monkhorst–Pack mesh k-space sampling grids with 3×3×6 k-point grids for all the models. For the convergence study of density of states (DOS), the much dense 5×5×6 k-point grids was set. The Cl-Cu_2O NC model was built using primitive cell of one Cl atom and 2×2 supercell of Cu_2O (1 0 0) with single layers (16 Cu atoms and 8 O atoms) as substrate. All the structures in this work were fully relaxed until the forces on each of the atoms were less than 0.02 eV/Å, and the self-consistency convergence criterion of energy is below 10^{-6} eV. To avoid the periodic interaction in the systems, a vacuum space of 20 Å was set in the direction normal to the surface.

Quantification of furandicarboxylic acid (FDCA)

For each HPLC measurement, quantitative electrolyte solution was sampled from the

electrochemical cell and diluted with 10 mM H_2SO_4 solution (to adjust the pH below 7.0), where 10 μL of the obtained mixture was injected into a BioRad Aminex 87H column afterward. 5 mM H_2SO_4 solution was used as the mobile phase in the isocratic mode with a constant flow rate (0.6 $mL \cdot min^{-1}$) at the column temperature of 40°C. A series of standard FDCA solutions with known concentrations were prepared, and their absorbance at 254 nm was measured to establish the calibration curve. The HMFOR products were identified by comparing the retention times of the HPLC elution peaks with the individual standard sample solutions. The product concentrations were calculated from the calibration curves using standard solutions.

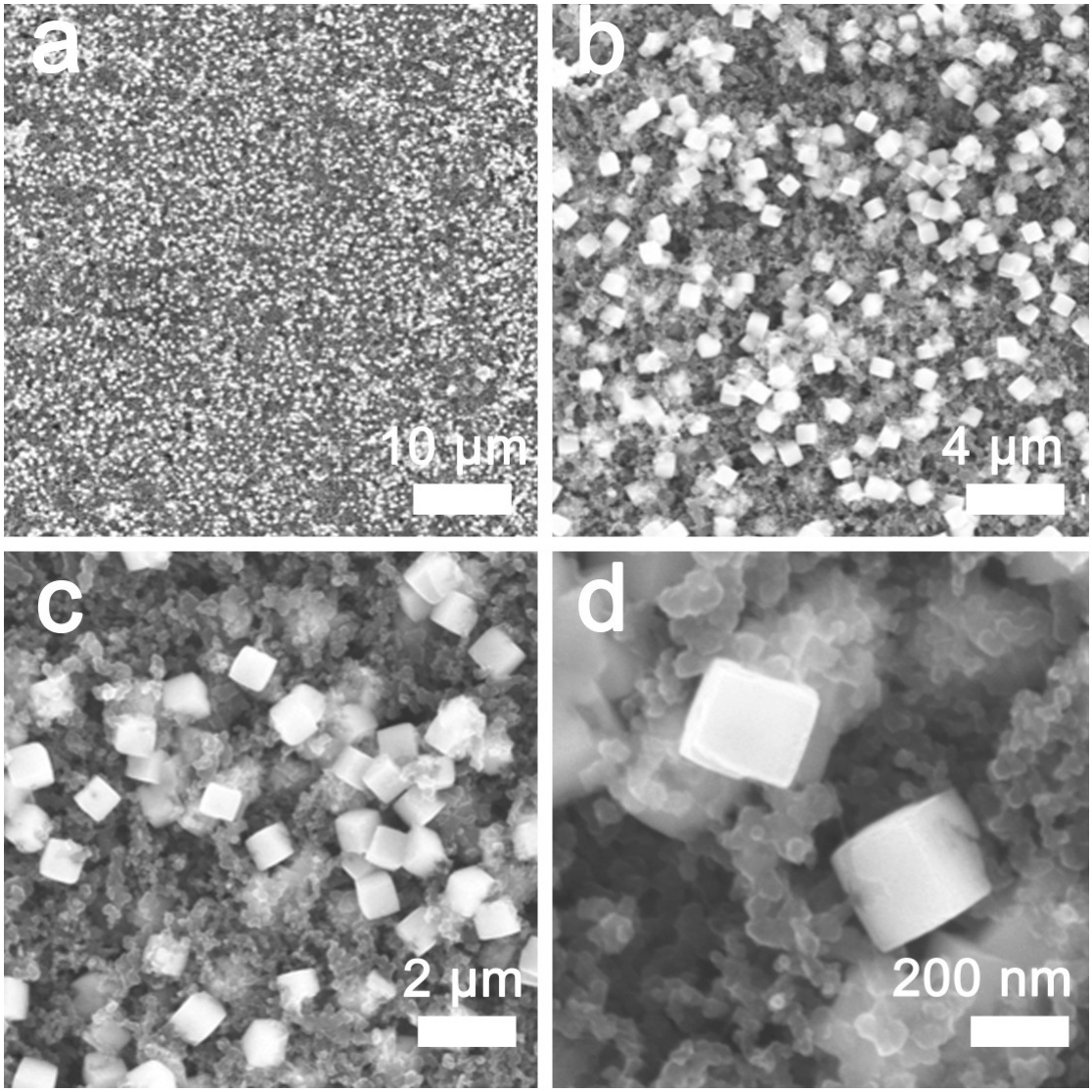

Figure S1. SEM images of Cl-Cu_2O NC loading on the carbon paper.

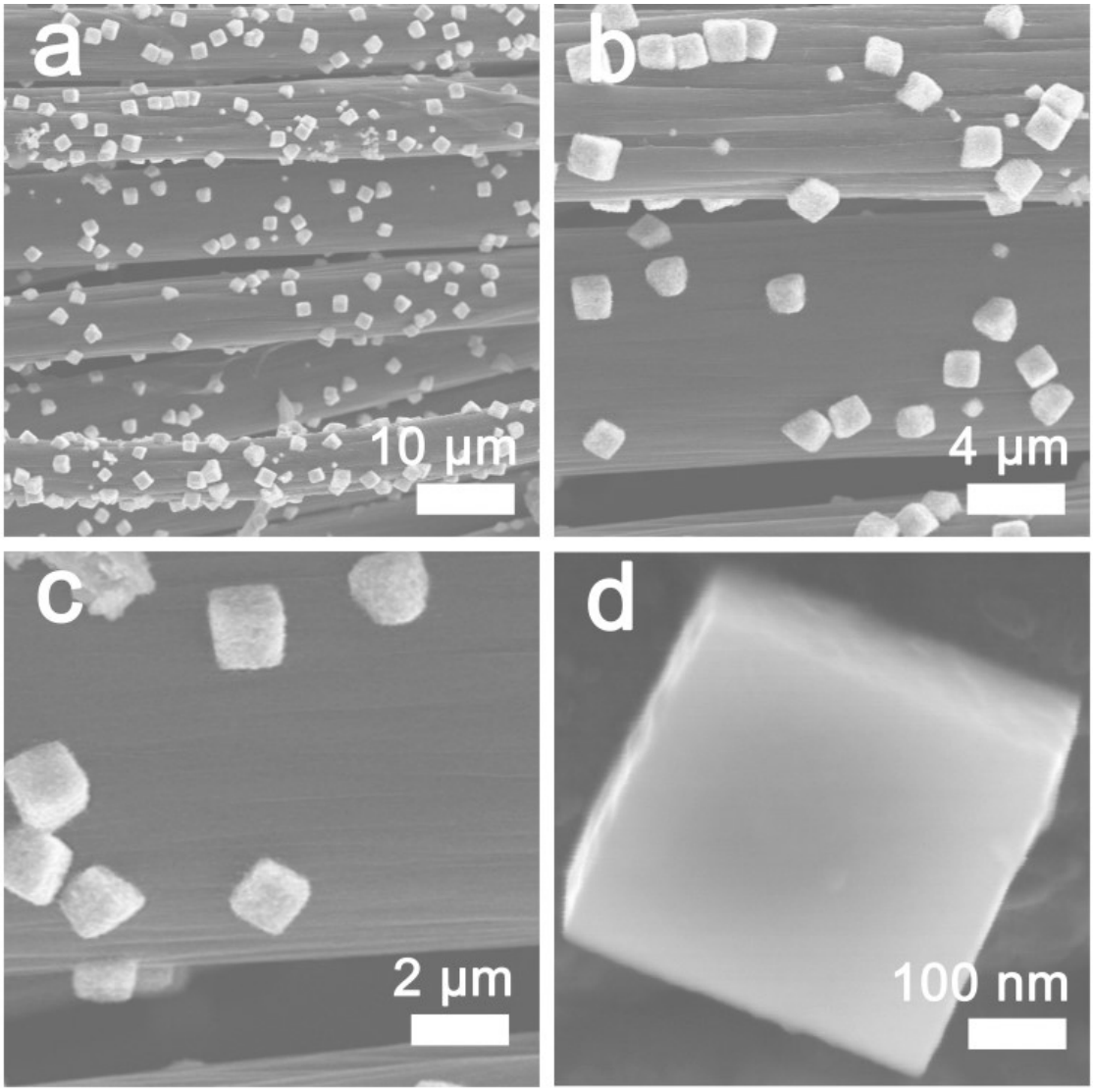

Figure S2. SEM images of Cl-Cu_2O NC loading on the carbon cloth.

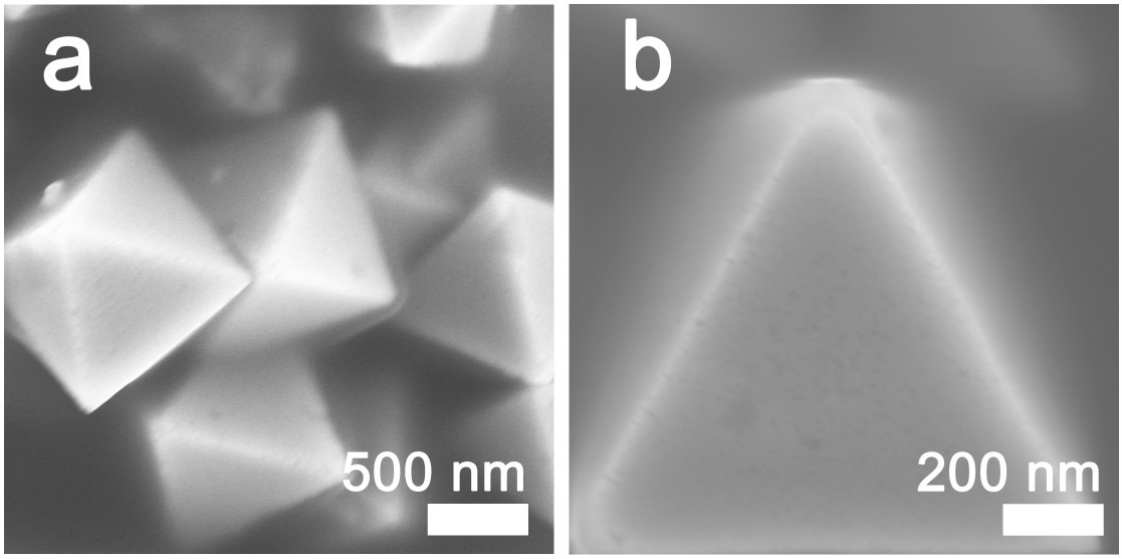

Figure S3. Low- (a) and high- (b) magnification of SEM images of Cu_2O Oct.

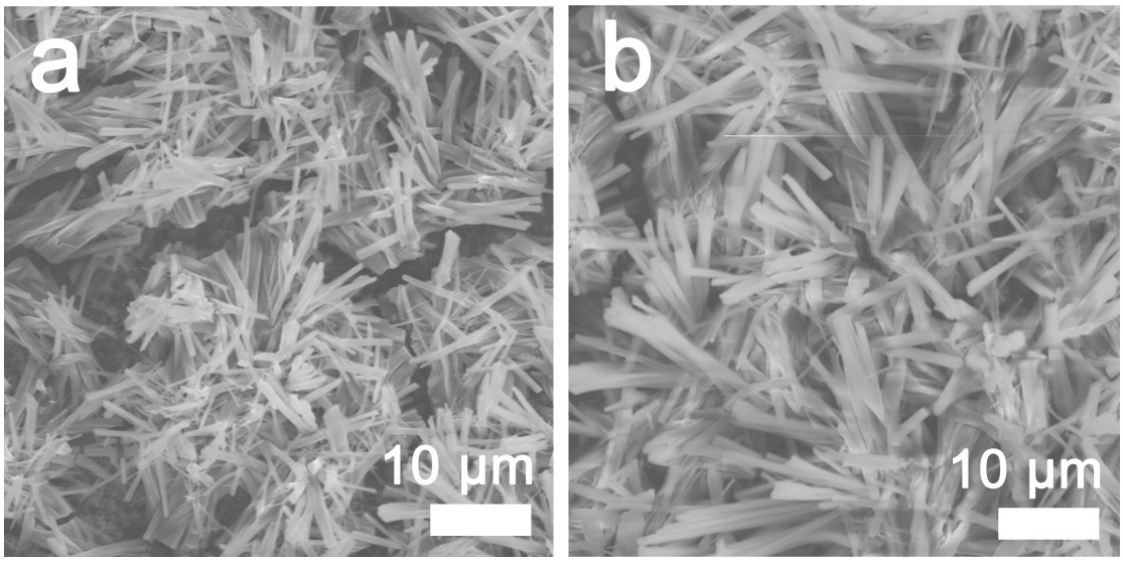

Figure S4. Low- (a) and high- (b) magnification of SEM images of $Cu(OH)_2$.

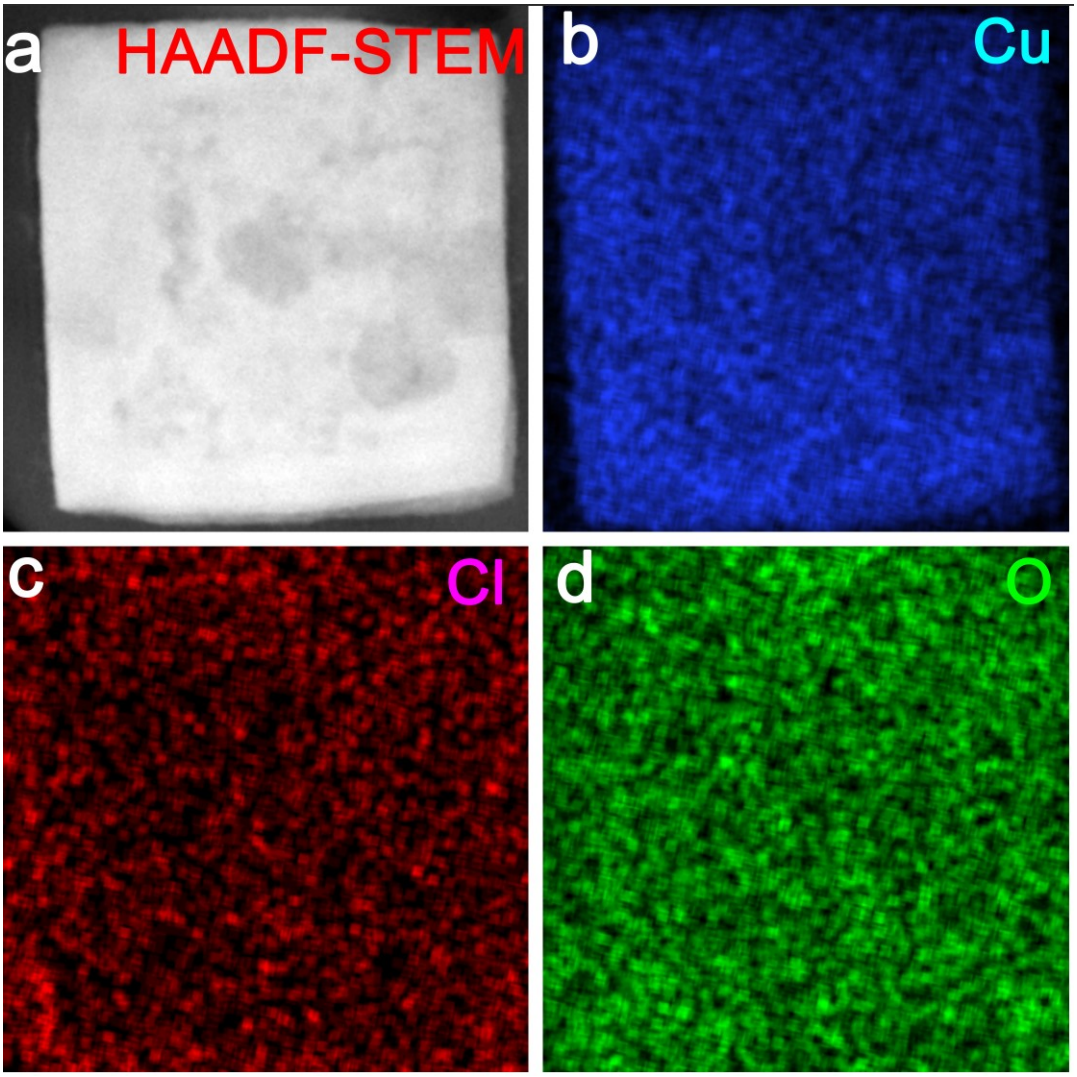

Figure S5. (a) HAADF-STEM images of Cl-Cu_2O NC. Elemental mapping images of (b) Cu, (c) Cl, and (d) O in Cl-Cu_2O NCs

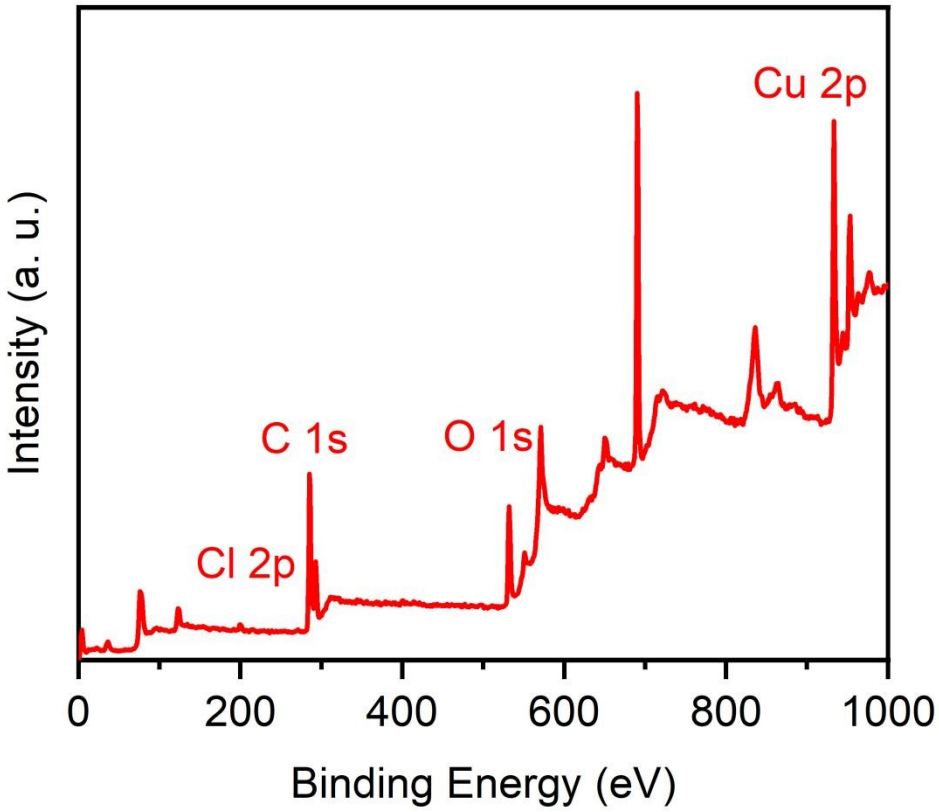

Figure S6. XPS survey spectra of Cl-Cu_2O NC.

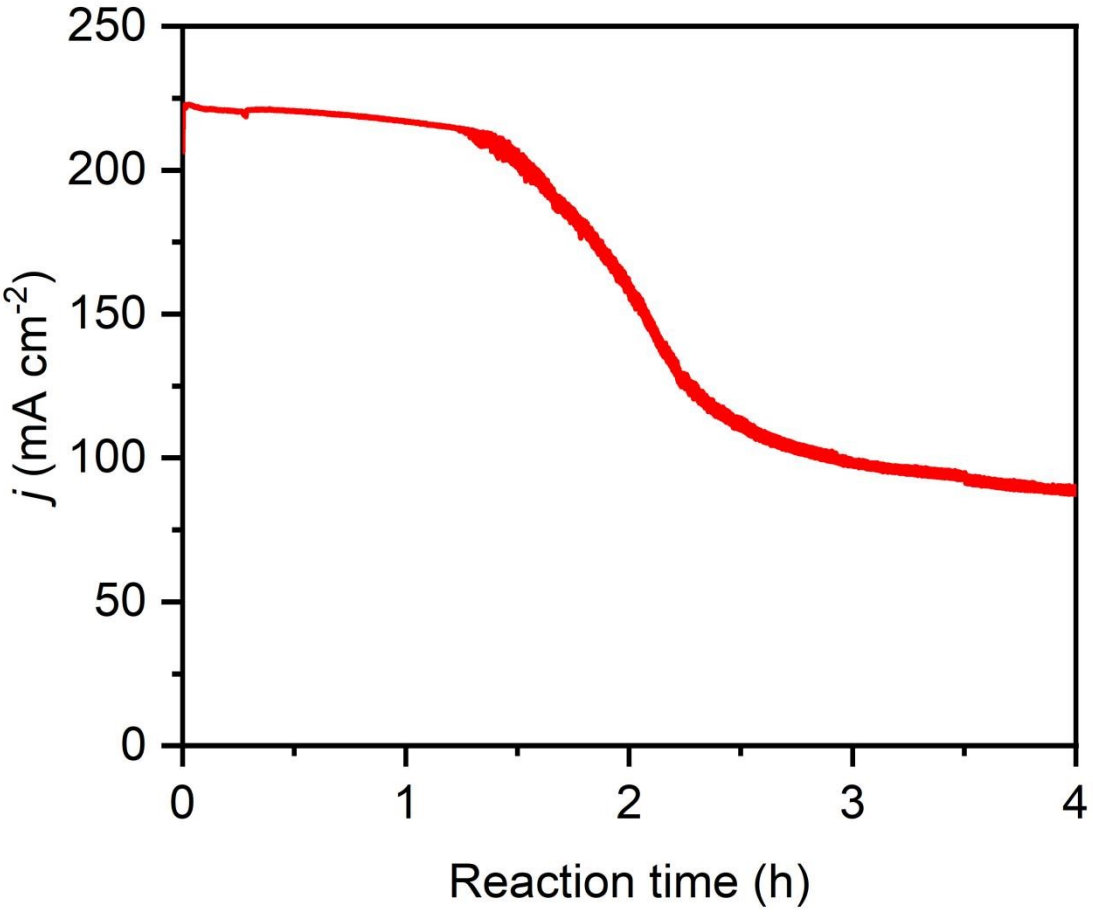

Figure S7. The it curves of HMFOR of Cl-Cu_2O.

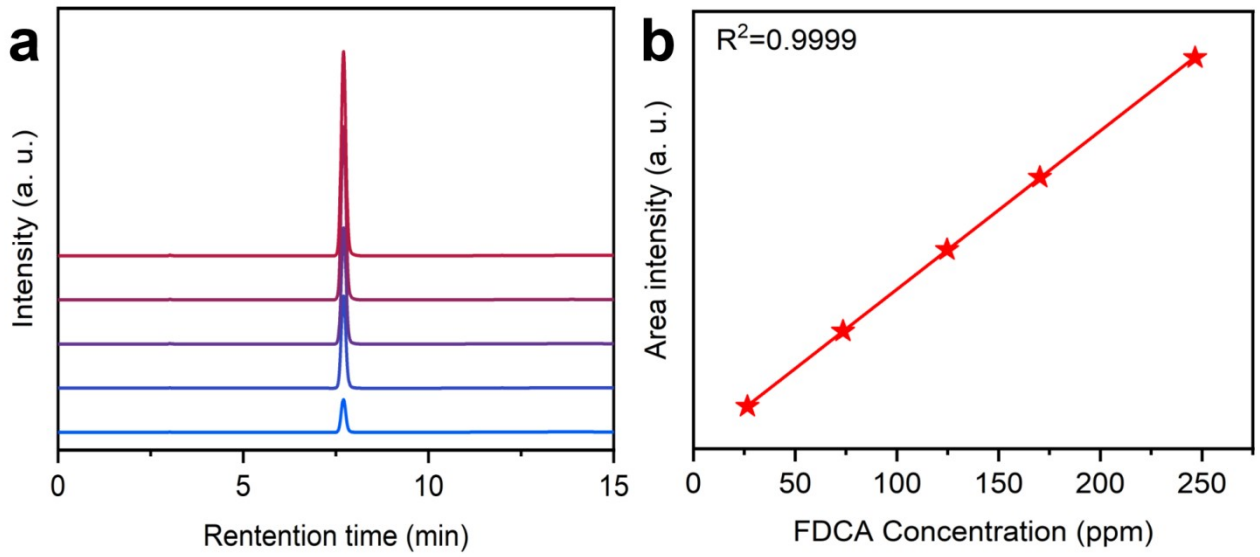

Figure S8. (a) HPLC spectra measured at different FDCA concentrations and (b) the calibration curves for confirmation of FDCA concentration.

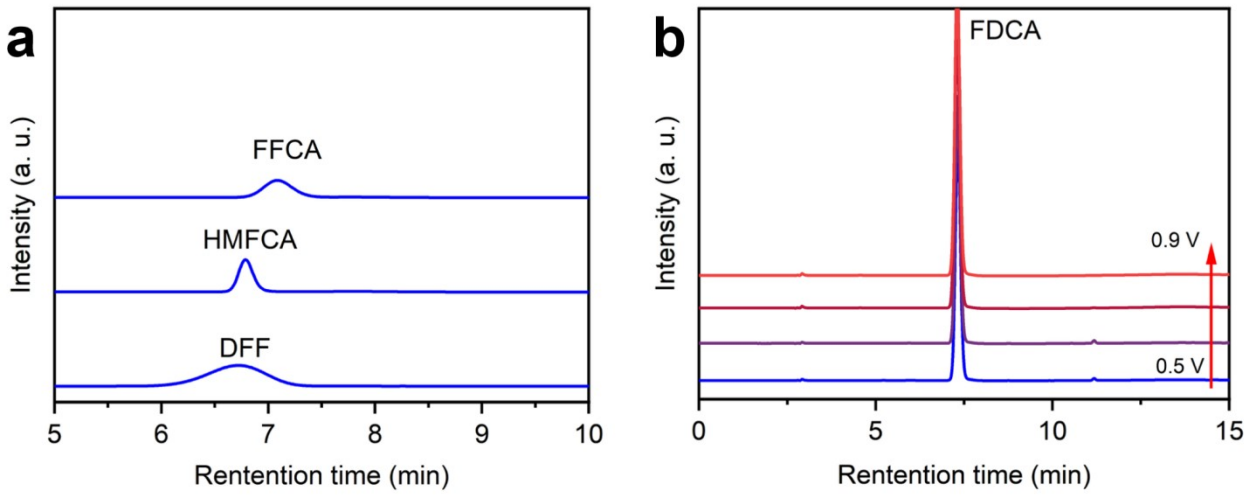

Figure S9. (a) HPLC spectra of the standard sample of intermediate products (DFF, HMFCA and FFCA). (b) Product distributions of HMF oxidation over Cl-Cu_2O NCs at different applied potentials.

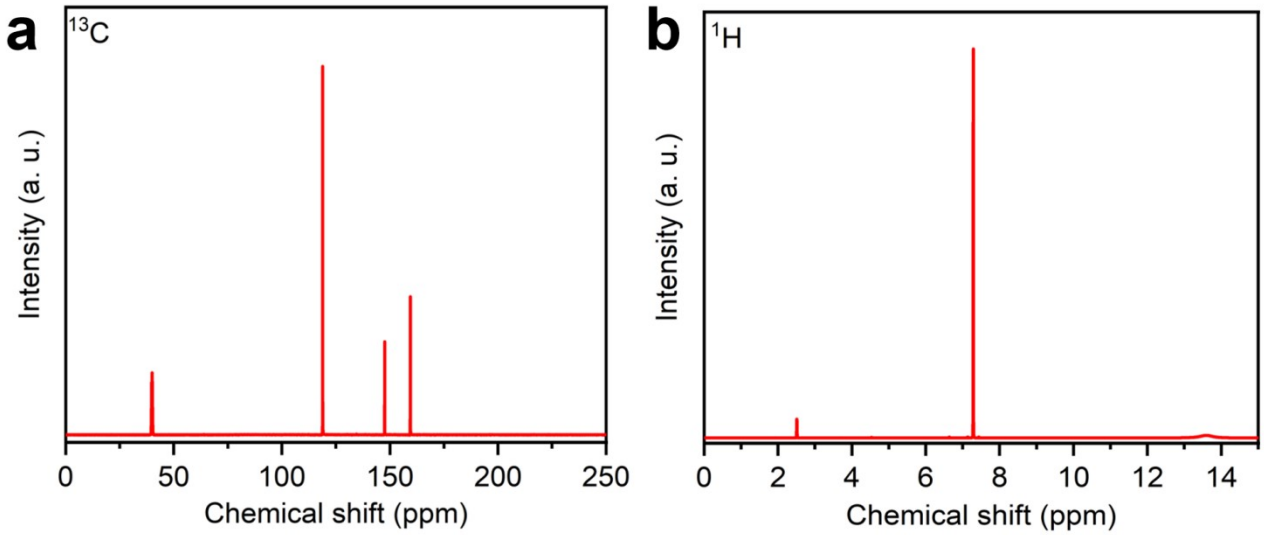

Figure S10. (a) ^{13}C-NMR spectra of the products. (b) ^{1}H-NMR spectra of the products.

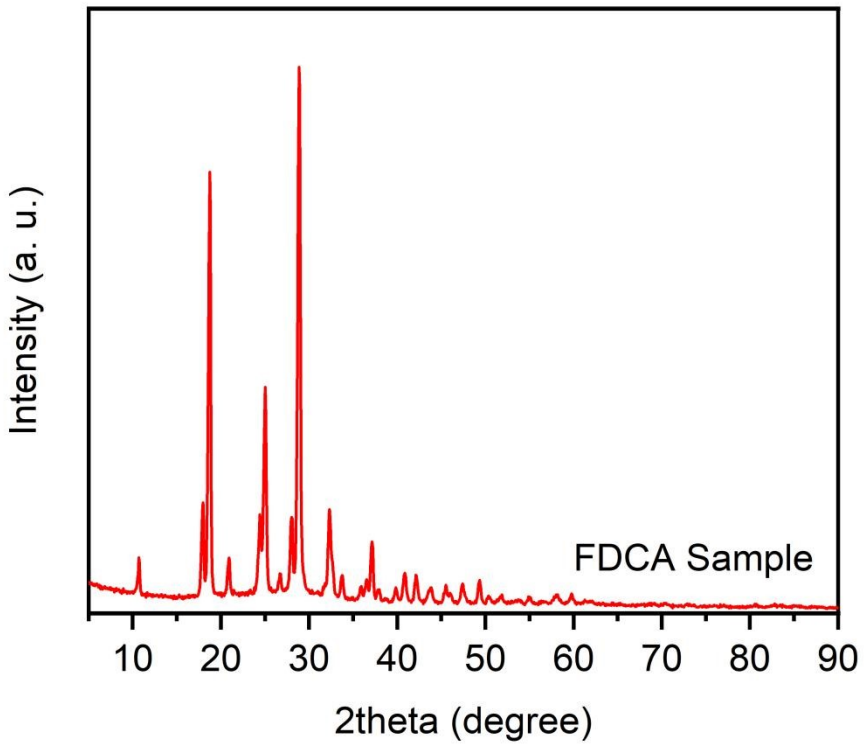

Figure S11. XRD pattern of the products.

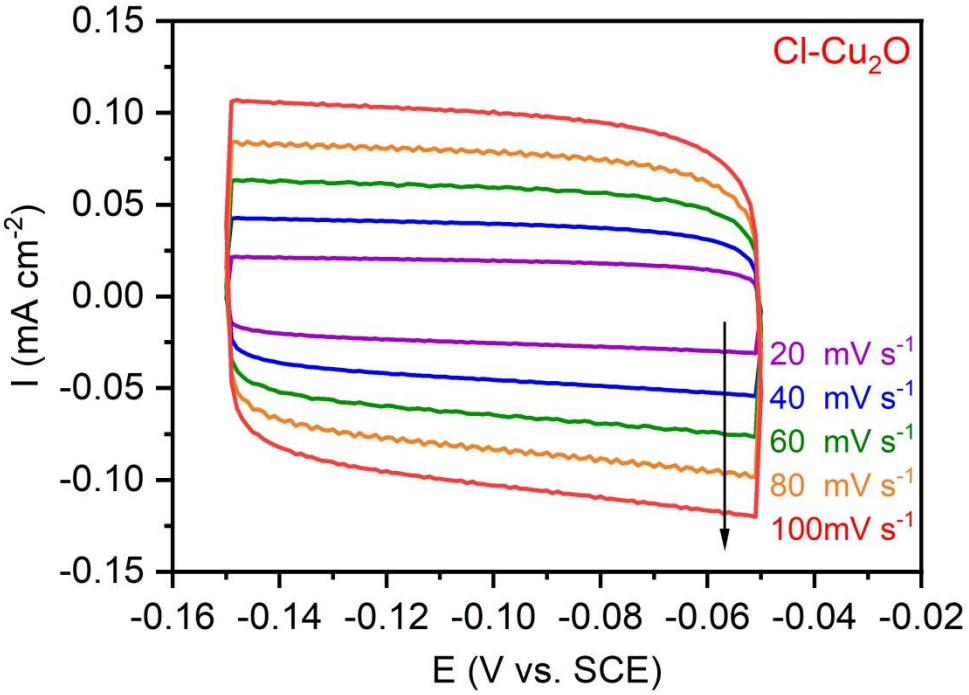

Figure S12. CVs curves of Cl-Cu_2O NC obtained in the voltage of -0.15~0.07 V at different scanning rates from 20 mV s^{-1} to 100 mV s^{-1} in 1 M KOH.

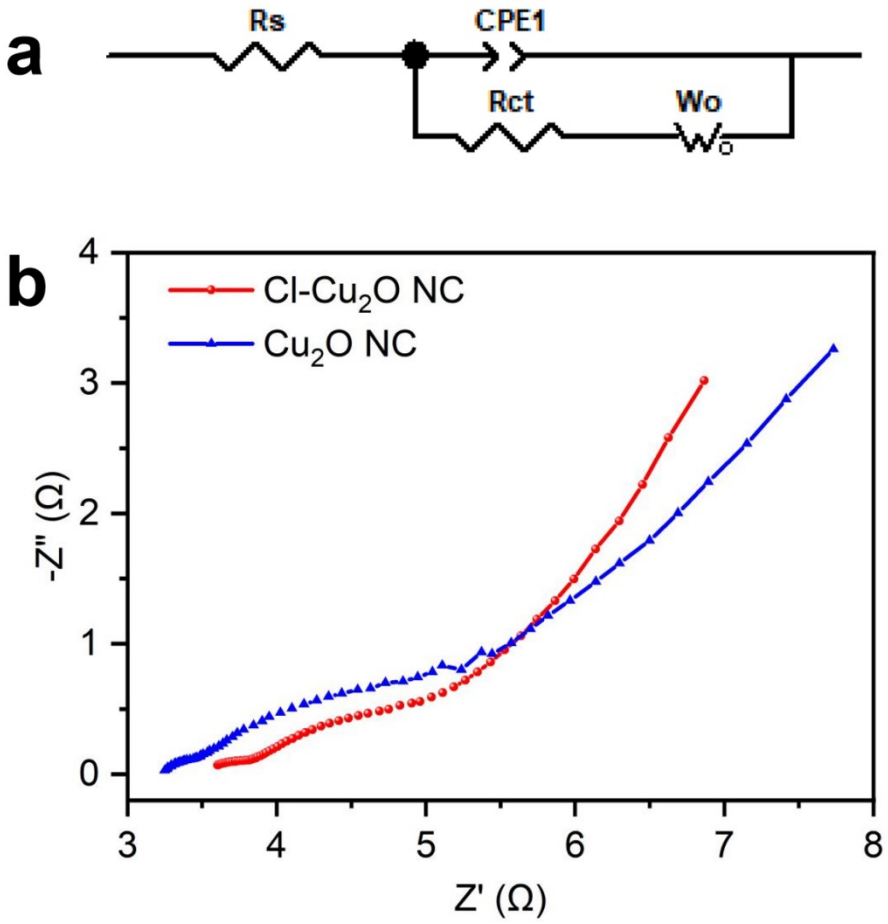

Figure S13. (a) Equivalent circuit diagram for EIS fitting. (b) Nyquist plots of pristine Cu_2O and Cl-Cu_2O NCs. The inset shows the equivalent circuit used for data fitting.

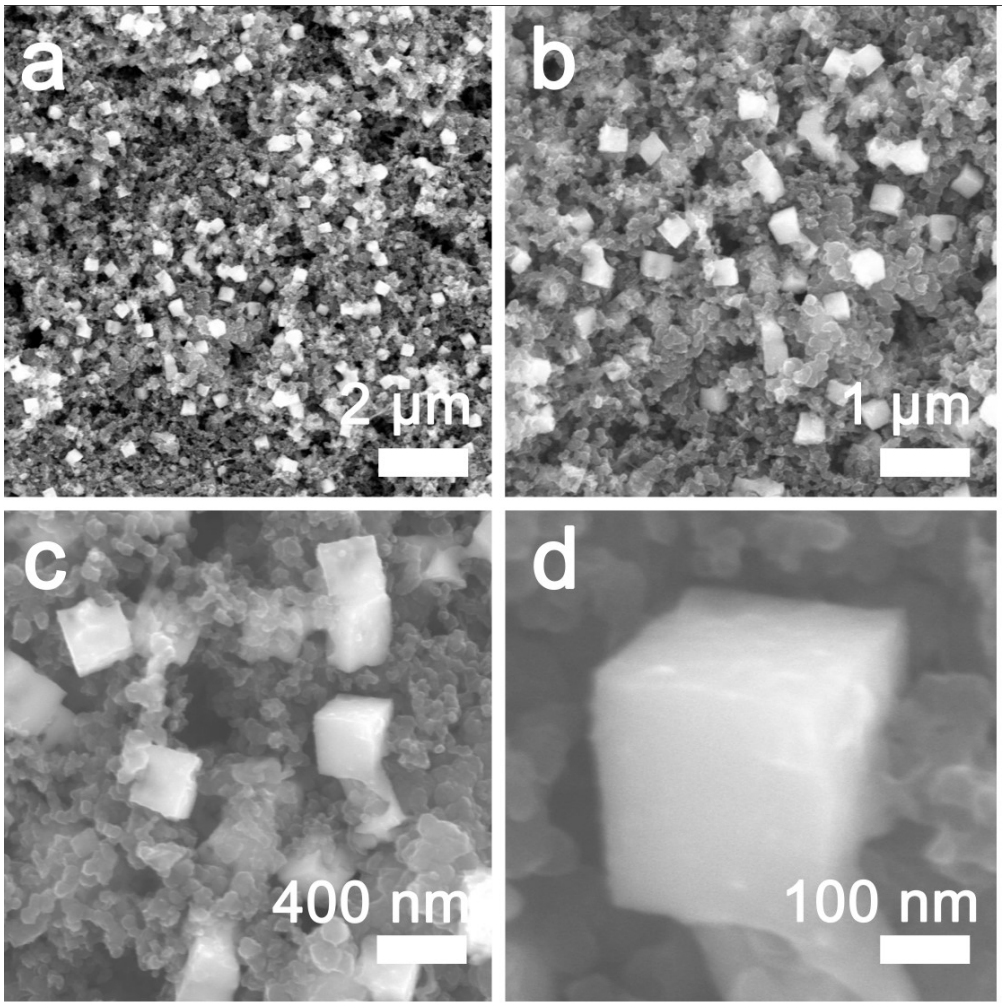

Figure S14. SEM images of Cl-Cu_2O NC after the electrochemical test.

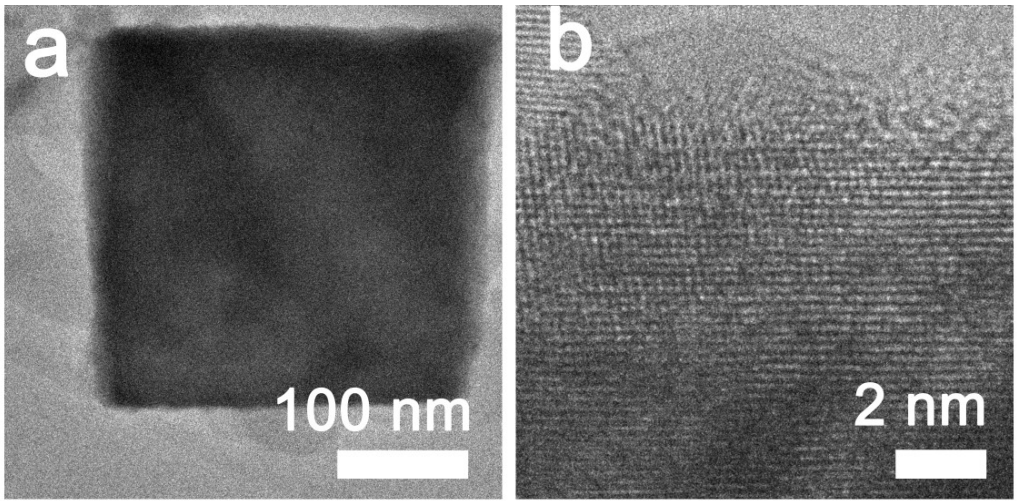

Figure S15. (a) TEM and (b) HRTEM of Cl-Cu_2O NC after the electrochemical test.

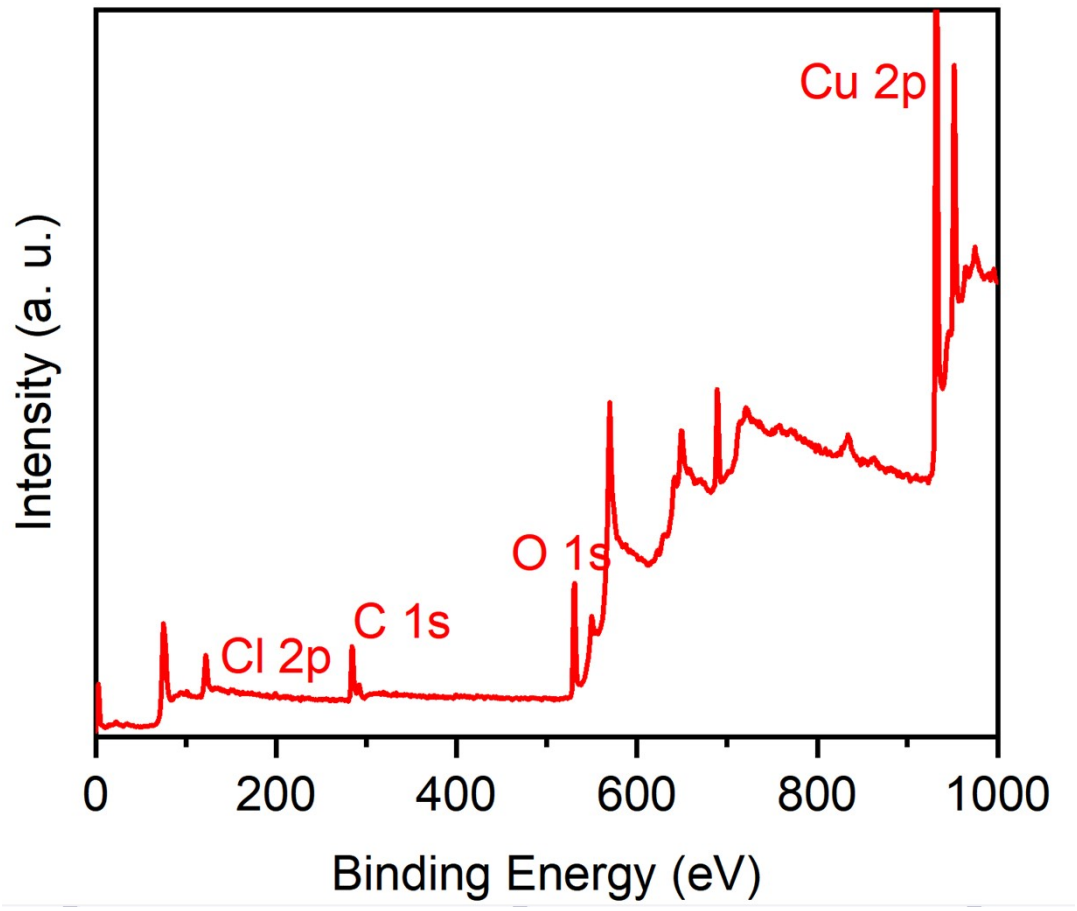

Figure S16. XPS survey spectra of Cl-Cu_2O NC after the electrochemical test.

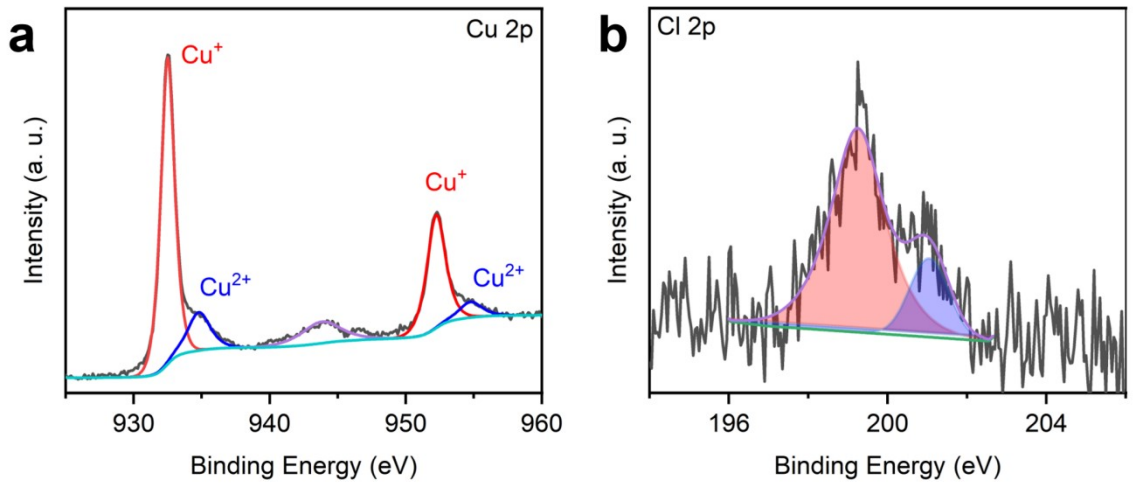

Figure S17. High-resolution (a) Cu 2p and (b) Cl 2p XPS spectra of Cl-Cu_2O NCs before and after the stability test.

Table S1. Element proportion of Cl-Cu_2O NC and Cu_2O NC according to the XPS results.

Sample	Element	Peak BE (eV)	Area (P) CPS. eV	Atomic Ratio %
Cl-Cu_2O NC	Cu	932.68	243583.66	59.28
	O	531.17	25991.12	35.23
	Cl	199.55	2546.37	5.49
Cu_2O NC	Cu	932.50	355356.34	63.41
	O	531.13	29591.58	36.59

Table S2. Fitted EIS parameters of pristine Cu_2O and Cl-Cu_2O NCs.

Sample	R_s (Ω)	Error (%)	R_{ct} (Ω)	Error (%)	Y_0 ($\Omega^{-1/2}$)	Error (%)
Cl-Cu_2O NC	3.71	0.005	2.88	0.076	0.086	0.0027
Cu_2O NC	3.32	0.007	3.68	0.093	0.054	0.0017

Table S3. The comparison in HMFOR performance with other reported catalysts.

Materials	Electrolyte	j (mA cm^{-2})	FE (%)	References
Cl-Cu_2O NC	100 mM HMF + 1 M KOH	200	97.9	This work
$(CoNiMnCuZn)_3O_4$	10 mM HMF + 1 M KOH	30	97.9	Nat. Commun. 15, 6761(2024)
Ag-$Co(OH)_2$	50 mM HMF + 1 M KOH	25	92.8	Adv. Mater., 2312402 (2024)
NiFe-LDH	100 mM HMF + 1 M KOH	200	98	ACS Catal. 8, 5533-5541 (2018).
Ni_3N@C	10 mM HMF + 1 M KOH	250	97.6	Angew. Chem. Int. Ed. 131, 16042-16050 (2019).
NiOOH/$Cu(OH)_2$	20 mM HMF + 1 M KOH	12	98.3	ACS Catal. 12, 4078-4091 (2022).
Vo-Co_3O_4	50 mM HMF + 1 M KOH	100	98.6	Adv. Mater. 34, 2107185 (2022)
MoO_2-FeP@C	10 mM HMF + 1 M KOH	10	91.9	Adv. Mater. 32, 2000455 (2020).
GDY/CuS_x	10 mM HMF + 1 M KOH	66	70	*Mater. Chem. Front.*, **7**, 2620 (2023)
Bi/GDY	10 mM HMF + 1 M KOH	19	91.7	*Chem. Res. Chinese Universities* **38**, 1380—1386 (2022)

Materials	Main product	j (mA cm^{-2})	FE (%)	References
Cl-Cu_2O NC	100 mM HMF + 1 M KOH	200	97.9	This work
Ir-Co_3O_4	50 mM HMF + 1 M KOH	10	98	Adv.Mater. 2021, 33, 2007056
Ni_3S_2/NF	10 mM HMF + 1 M KOH	50	98	J. Am. Chem. Soc. 2016, 138, 13639-13646.
NiFe LDH	100 mM HMF + 1 M KOH	200	98	ACS Catal. 2018, 8, 5533-5541
$CuCo_2O_4$	50 mM HMF + 1 M KOH	225	93.7	Angew. Chem., Int. Ed. 2020, 59, 19215-19221
High-Entropy Oxide Nanosheets	50 mM HMF + 1 M KOH	44	94	Angew. Chem., Int. Ed. 2021, 60, 20253-20258.
Vo-Sc_2O_3	10 mM HMF + 1 M KOH	~10	>96%	Adv. Mater. 2024, 36, 2311698
MoO_2-FeP@C	10 mM HMF + 1 M KOH	10	98.6	Adv. Mater. 2020, 32, 2000455
NiMn UT-LDHs	10 mM HMF + 1 M KOH	20	92.7	Adv. Mater. 2023, 35, 2305573
Ag-$Co(OH)_2$	50 mM HMF + 1 M KOH	26	92.8	Adv. Mater. 2024, 36, 2312402
CoO_xH_y	50 mM HMF + 1 M KOH	30	81.2	Angew. Chem. Int. Ed. 2021, 60, 20535 – 20542
Ir-Co_3O_4	50 mM HMF + 1 M KOH	10	98	Adv.Mater. 2021, 33, 2007056
Ni_3S_2/NF	10 mM HMF + 1 M KOH	50	98	J. Am. Chem. Soc. 2016, 138, 13639-13646.